Inorganic Chemistry

Article

pubs.acs.org/IC

$Sc_2O@C_{2v}(5)$-C_{80}: Dimetallic Oxide Cluster Inside a C_{80} Fullerene Cage

Qiangqiang Tang,[†] Laura Abella,[§] Yajuan Hao,[‡] Xiaohong Li,[†] Yingbo Wan,[†] Antonio Rodríguez-Fortea,*[,§] Josep M. Poblet,*[,§] Lai Feng,*[,‡] and Ning Chen*[,†]

[†]Laboratory of Advanced Optoelectronic Materials, College of Chemistry, Chemical Engineering and Materials Science, Soochow University, Suzhou, Jiangsu 215123, China

[‡]College of Physics, Optoelectronics and Energy & Collaborative Innovation Center of Suzhou Nano Science and Technology, Soochow University, Suzhou 215006, China

[§]Departament de Química Física i Inorgànica, Universitat Rovira i Virgili, c/Marcel·lí Domingo 1, 43007 Tarragona, Spain

Supporting Information

ABSTRACT: A new oxide cluster fullerene, $Sc_2O@C_{2v}(5)$-C_{80}, has been isolated and characterized by mass spectrometry, UV−vis−NIR absorption spectroscopy, cyclic voltammetry, ^{45}Sc NMR, DFT calculations, and single crystal X-ray diffraction. The crystallographic analysis unambiguously elucidated that the cage symmetry was assigned to $C_{2v}(5)$-C_{80} and suggests that the Sc_2O cluster is ordered inside the cage. The crystallographic data further reveals that the Sc1−O−Sc2 angle is much larger than that found in $Sc_2O@T_d(19151)$-C_{76} but almost comparable to that in $Sc_2O@C_s(6)$-C_{82}, suggesting that the endohedral Sc_2O unit is flexible and can display large variation in the Sc−O−Sc angle, which depends on the size and shape of the cage. Computational studies show that there is a formal transfer of four electrons from the Sc_2O unit to the C_{80} cage, i.e., $(Sc_2O)^{4+}@(C_{80})^{4-}$, and the HOMO and LUMO are mainly localized on the C_{80} framework. Moreover, thermal and entropic effects are seen to be relevant in the isomer selection. Comparative studies between the recently reported $Sc_2C_2@C_{2v}(5)$-C_{80} and $Sc_2O@C_{2v}(5)$-C_{80} reveal that, despite their close structural resemblance, subtle differences exist on the crystal structures, and the clusters exert notable impact on their spectroscopic properties as well as interactions between the clusters and corresponding cages.

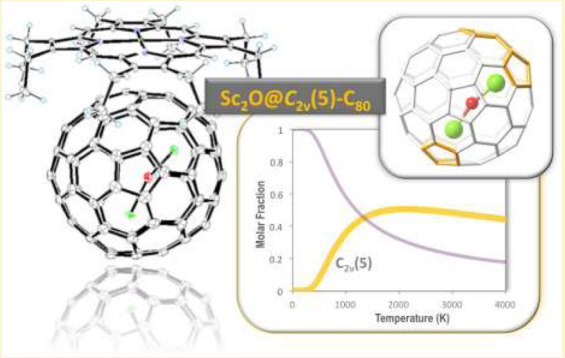

INTRODUCTION

Endohedral fullerenes, featured by the encapsulation of metal ions, molecules, and clusters inside the hollow sphere of carbon cage, have attracted special interest in the fullerene research field ever since the first successful extraction of $La@C_{82}$ in 1991.[1−8] One of the fascinating characters of these compounds is the fact that their physical and chemical properties as well as electronic structures can be fine-tuned by the variable species encapsulated inside fullerene cages.[7,9−11] This unique property has generated broad interest over potential applications in the field of biomedicines, molecular electronic devices, catalysis, and solar cells.[9,12−16]

The interaction between the carbon cages and entrapped clusters has been the focus of endohedral fullerene studies.[17] It has been revealed that this cage−cluster interaction has an essential impact on the structure and chemical properties of endohedral fullerenes.[18] The electron transfer from the cluster to cage and structural matching between them largely determine that, for a certain cluster, which kind of cage symmetry will be selected out of hundreds or thousands of possibilities.[19,20] Moreover, this interaction can stabilize not only the cages and but also the endohedral clusters which are otherwise unstable.[9] For example, isomeric cages of C_{80} are popular cages for various forms of endohedral fullerenes.[21] However, one of them, $C_{2v}(5)$-C_{80}, remained missing until its recent discovery by Akasaka et al. in the study of $Sc_2C_2@C_{2v}(5)$-C_{80}.[22] It was found that this cage structure was stabilized by a four-electron-transfer from the encapsulated Sc_2C_2 cluster. To our best knowledge, this is the only fullerene with $C_{2v}(5)$-C_{80} reported so far.

Similar to the carbide cluster fullerenes, oxide cluster fullerenes (OCFs) demonstrate structural varieties of encapsulated oxide clusters, i.e., $Sc_4O_2@C_{80}$[15,23,24] and $Sc_4O_3@C_{80}$.[25] Most OCFs have been found to be encapsulated in the $I_h(7)$-C_{80} cage with a six-electron cluster-cage charge transfer, with the only exception of a dimetallic OCF, $Sc_2O@C_s(6)C_{82}$.[26] Very recently, we reported the synthesis of an extensive dimetallic OCFs family (i.e., $Sc_2O@C_{2n}$, n = 35−47).[27] This new OCF family, on the other hand, presents interesting structural varieties of fullerene cages, which offer unique opportunities to understand the interactions between the dimetallic clusters and different cages as well as the structural correlations between these cages.[27] Among them, $Sc_2O@T_d(19151)$-C_{76} and $Sc_2O@C_2(7892)$-C_{70} have been isolated and fully characterized.[27,28] Herein, we report a new OCF,

Received: July 18, 2015
Published: September 30, 2015

DOI: 10.1021/acs.inorgchem.5b01613
Inorg. Chem. 2015, 54, 9845−9852

$Sc_2O@C_{80}$. A combined study of UV−vis−NIR absorption, single crystal X-ray characterization and DFT calculations unambiguously assigned the cage structure to $C_{2v}(5)$-C_{80}, the first OCF with a C_{80} cage different from the prototypical $I_h(7)$-C_{80}. Furthermore, we compared the spectroscopic and electrochemical properties of this molecule to the previously reported $Sc_2C_2@C_{2v}(5)$-C_{80}. The results show that, though the two species share the same cage as well as the similar electronic structure of $(Sc_2M)^{4+}@(C_{2v}(5)\text{-}C_{80})^{4-}$ (M = O or C_2), they demonstrate different spectroscopic and electrochemical properties, indicating a notable impact from the endohedral clusters.

RESULTS AND DISCUSSION

Preparation and Purification. The OCFs were synthesized in a conventional Krätschmer−Huffman arc-discharge reactor under a He/CO_2 (10:1) atmosphere. The soot was collected and refluxed in chlorobenzene under an argon atmosphere for 24 h. A multistage high performance liquid chromatography (HPLC) procedure was used to isolate and purify $Sc_2O@C_{80}$ (see Figures S1 and S2).

In our study, $Sc_2O@C_{80}$ ranks as the fourth most abundant OCF after $Sc_2O@C_{82}$, $Sc_2O@C_{78}$, and $Sc_2O@C_{76}$. The rough yield of this product is estimated to be around 20% of that of the $Sc_2O@C_{82}$. The MALDI-TOF spectrum of the purified sample shows a single peak at 1065.986 m/z. This molecular weight and the isotopic distribution of the experimental MALDI spectrum agree very well with the corresponding theoretical simulation (see Figure 1).

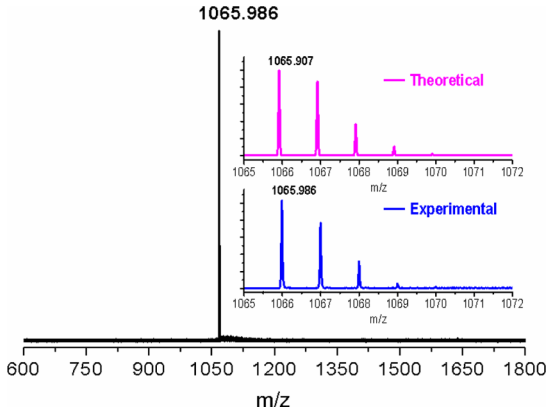

Figure 1. Mass spectra of the purified $Sc_2O@C_{80}$. Inset: Experimental and theoretical isotopic distributions for $Sc_2O@C_{80}$.

Structure of $Sc_2O@C_{2v}(5)$-C_{80} As Determined by Single Crystal X-ray Diffraction. The structure of $Sc_2O@C_{80}$ was characterized via a single crystal X-ray diffraction (XRD) study. Cocrystals of $Sc_2O@C_{80}/[Ni^{II}(OEP)]$ suitable for X-ray analysis were obtained by slow diffusion of a benzene solution of $Sc_2O@C_{80}$ into a $CHCl_3$ solution of $[Ni^{II}(OEP)]$. The molecular structure was resolved and refined in a $C2/m$ (No. 12) space group. Figure 2 shows the X-ray structure of this OCF, and its relationship with the adjacent $[Ni^{II}(OEP)]$ moiety. The crystallographic data clearly suggest a $C_{2v}(5)$-C_{80} cage with an endohedral Sc_2O cluster. Particularly, the $C_{2v}(5)$-C_{80} cage is disordered in two orientations with fractional occupancies of 0.421 and 0.079, respectively, and only the major orientation is shown in Figure 2. The porphyrin moiety tends to approach the flat region of $C_{2v}(5)$-C_{80} cage with the shortest nickel-to-cage carbon distance of 2.744(6) Å, suggesting a large $\pi-\pi$ stacking interaction between the fullerene and porphyrin moiety.

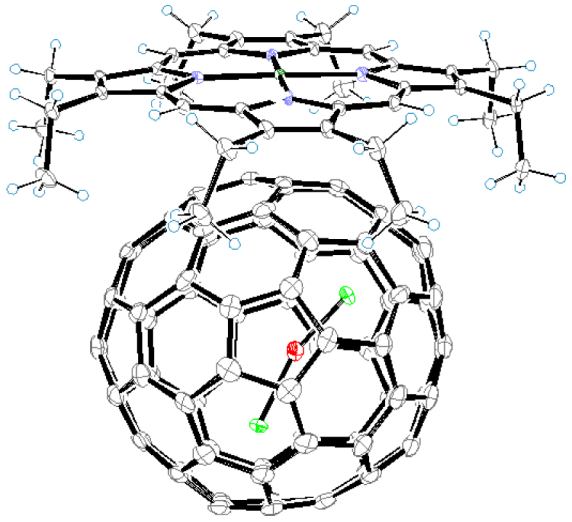

Figure 2. ORTEP drawing of $Sc_2O@C_{2v}(5)$-$C_{80}/[Ni^{II}(OEP)]$ with 30% thermal ellipsoids, showing the relationship between the fullerene cage and $[Ni^{II}(OEP)]$. Only the major cage orientation with 0.421 occupancy and the major Sc_2O unit with the same occupancy are shown. For clarity, the solvent molecules, minor cage orientation, and minor Sc_2O unit are omitted.

Inside the fullerene cage, although only one oxygen site is identified, the Sc atoms are found to be disordered over four positions, which can be paired into two sets according to their occupancies, matching well with those of major and minor cage orientations, respectively. Particularly, Sc1 and Sc2 sites are assigned to the major cage, while Sc3 and Sc4 are assigned to the minor cage. In the major Sc_2O unit, the Sc−O distances are 1.861(4) Å for Sc1 and 2.017(4) Å for Sc2, similar to the Sc−O distances reported for $Sc_2O@T_d(19151)$-C_{76} and $Sc_2O@C_s(6)$-C_{82}. It is noteworthy that the Sc1−O−Sc2 angle is 160.79(18)°, much larger than that found in $Sc_2O@T_d$-C_{76} (i.e., 133.9(4)°) but almost comparable to that in $Sc_2O@C_s(6)$-C_{82} (i.e., 156.6(3)°). These results suggest that the endohedral Sc_2O unit is flexible and can display large variation in the Sc−O−Sc angle, which might depend on the size and shape of the cage.

However, due to the crystallographic mirror plane being mismatched with the molecular symmetry, the crystallographic data alone cannot determine the relative orientation between the Sc_2O cluster and cage. In fact, inside the major cage, either the major cluster shown in Figure 2 or that generated via the crystallographic mirror plane is equally suggested by X-ray analysis. Theoretical calculations are employed to determine that the absolute structure of $Sc_2O@C_{2v}(5)$-C_{80} is the one shown in Figure 2.

Spectroscopic Characterization: UV−Vis−NIR and ^{45}Sc NMR. The purified sample presents a deep brown color in CS_2 solution. Figure 3 shows that the overall absorption pattern of $Sc_2O@C_{2v}(5)$-C_{80} closely resembles that of the $Sc_2C_2@C_{2v}(5)$-C_{80}.[22] Both of the spectra are featured by major absorptions at ca. 650 and 800 nm. Since the UV−vis−NIR absorption has been universally acknowledged as the fingerprint signature to the assignment of the fullerene cages and their electronic structures, these results verified that the cage symmetry of $Sc_2O@C_{80}$ is identical to that of the $Sc_2C_2@C_{2v}(5)$-C_{80}. However, despite the overall resemblance, some notable

DOI: 10.1021/acs.inorgchem.5b01613
Inorg. Chem. 2015, 54, 9845−9852

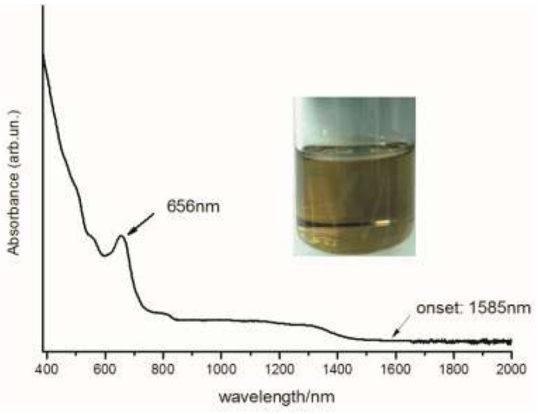

Figure 3. UV−vis−NIR spectrum of $Sc_2O@C_{2v}(5)$-C_{80} in CS_2; inset shows the color of $Sc_2O@C_{2v}(5)$-C_{80} in CS_2 solution.

differences have also been observed in two absorption spectra. Particularly, while the absorption spectrum of $Sc_2C_2@C_{2v}(5)$-C_{80} demonstrates a triplet absorption peak at 656 nm, $Sc_2O@C_{2v}(5)$-C_{80} shows a singlet absorption peak. Additionally, the minor absorption peak at 558 nm in the spectrum of $Sc_2O@C_{2v}(5)$-C_{80} is not visible in the same absorption range in the spectrum of $Sc_2C_2@C_{2v}(5)$-C_{80}. The different endohedral clusters likely cause these differences. These differences suggest that, though sharing the same cage and electronic structure, the cluster-cage interactions in $Sc_2O@C_{2v}(5)$-C_{80} and $Sc_2C_2@C_{2v}(5)$-C_{80} are somewhat different, which leads to a noticeable impact on the energy distribution of frontier MO and hence the excitation spectra. The absorption onset of $Sc_2O@C_{2v}(5)$-C_{80} is around 1585 nm, suggesting an optical gap of 0.78 eV. Optical gap roughly corresponds to the HOMO−LUMO gap and shows if a molecule is kinetically stable or not. Using 1.0 eV as the limit to distinguish large and small bandgap, we can assign $Sc_2O@C_{2v}(5)$-C_{80} as small bandgap molecule. This band gap is very close to 0.79 eV for $Sc_2O@T_d(19151)$-C_{76}.

The ^{45}Sc NMR spectrum of $Sc_2O@C_{2v}(5)$-C_{80} is presented in Figure 4. The single line at 39.2 ppm was recorded at 298 K, which agrees with DFT simulations that the Sc_2O cluster rotates at this temperature (*vide infra*). This result also suggests that the Sc_2O cluster inside $Sc_2O@C_{2v}(5)$-C_{80} shows different dynamic motions from those of the Sc_2C_2 inside $Sc_2C_2@C_{2v}(5)$-C_{80}, in which Sc_2C_2 remains fixed at 298 K and the ^{45}Sc

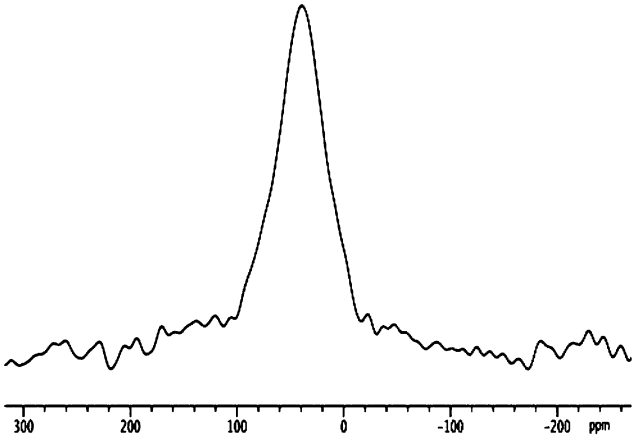

Figure 4. ^{45}Sc NMR spectrum of $Sc_2O@C_{2v}(5)$-C_{80} at room temperature.

spectrum of $Sc_2C_2@C_{2v}(5)$-C_{80} shown a broad doublet signal at this temperature.[29] On the other hand, the comparison of ^{45}Sc NMR spectra within the oxide cluster fullerene family suggests that the chemical shifts of Sc atoms are very sensitive to the cage size and symmetry, as it shifts from 76.9 ppm for $Sc_2O@T_d(19151)$-C_{76} to 39.2 ppm for $Sc_2O@C_{2v}(5)$-C_{80}.[28]

Electrochemical Studies. The electrochemical properties of $Sc_2O@C_{2v}(5)$-C_{80} were investigated by cyclic voltammetry (CV) (Table 1). The CV of $Sc_2O@C_{2v}(5)$-C_{80} shows five reduction peaks and two oxidation peaks (Figure 5). The oxidation processes are completely reversible, which is similar to other OCFs.[15,26,27] On the contrary, the reduction processes are irreversible. In general, this overall redox pattern shows much greater resemblance to the CV of $Sc_2C_2@C_{2v}(5)$-C_{80} than to that of $Sc_2O@T_d(19151)$-C_{76} and $Sc_2O@C_s(6)$-C_{82}, suggesting its frontier orbitals are more related to cage rather than the encapsulated cluster (frontier orbitals are mainly localized on the cage, *vide infra*). Interestingly, this result is very different from what was observed in the comparative study of $Sc_2O@C_s(6)$-C_{82} and $Sc_2S@C_s(6)$-C_{82}, in which the overall redox patterns of two molecules show significant differences despite the structural resemblance of the encapsulated Sc_2O and Sc_2S. However, the first reduction potential and oxidation potential of $Sc_2O@C_{2v}(5)$-C_{80} notably shift by −0.17 and −0.15 V compared to those of the $Sc_2C_2@C_{2v}(5)$-C_{80}, indicating the considerable impact of the different clusters on the frontier orbitals of the cluster fullerenes. This trend is again in contrast to what we found for the comparison between $Sc_2O@C_s(6)$-C_{82} and $Sc_2S@C_s(6)$-C_{82}, in which the first reduction potentials and oxidation potentials of these two molecules are very close to each other and variations of redox potentials of these two structures are within 0.05 V. The electrochemical gap of $Sc_2O@C_{80}$ is 1.13 V, which is almost identical to that of $Sc_2C_2@C_{2v}(5)$-C_{80} (1.15 V) but smaller than those of other OCFs discovered so far.

Computational Studies. Besides the experimental characterization of $Sc_2O@C_{2v}(5)$-C_{80}, our computations confirmed that the $C_{2v}(5)$-C_{80} cage is the most favored isomer to encapsulate the Sc_2O cluster. For a C_{80} cage there are 31 924 isomers, but only seven of them follow the isolated pentagon rule (IPR). We assume that a formal transfer of four electrons takes place from the cluster to the cage, as for $Sc_2O@C_{82}$ (the orbital interaction diagram will confirm such an assumption, *vide infra*). First, we have computed the energies of the tetra-anions using DFT at BP86/TZP level for all cages with two or fewer adjacent pentagon pairs (APP): 7 IPR isomers, 36 APP1 isomers, and 415 APP2 isomers. The lowest-energy tetra-anionic cages (less than 40 kcal mol^{-1}) were selected, and the corresponding structures of $Sc_2O@C_{80}$ were optimized at the same BP86/TZP level. Different orientations of the Sc_2O cluster in IPR cages were taken into account. The IPR cage $I_h(7)$-C_{80} was found to be the lowest-energy tetra-anion, with isomers 6 and 5 within a range of less than 10 kcal mol^{-1}. However, an energy inversion within the IPR isomers is observed when the Sc_2O cluster is encapsulated. In particular, $Sc_2O@D_{5h}(6)$-C_{80} is found to be the lowest-energy OCF, followed by isomers 5 and 7 with relative energies smaller than 4 kcal mol^{-1} (Table 2). The non-IPR OCFs with one or two APPs show significantly higher energies than the IPR isomers. Cages $C_{2v}(5)$-C_{80}, $D_{5h}(6)$-C_{80}, and $I_h(7)$-C_{80} show the lowest number of pyracylenes within the IPR subset and the smallest electrostatic contributions to the bond energies, as usually

DOI: 10.1021/acs.inorgchem.5b01613
Inorg. Chem. 2015, 54, 9845−9852

Table 1. Redox Potentials (V vs Fc^+/Fc) of $Sc_2O@C_{2v}(5)$-C_{80}, $Sc_2C_2@C_{2v}(5)$-C_{80},[22] $Sc_2O@C_s(6)$-C_{82},[26] $Sc_2S@C_s(6)$-C_{82},[30] and $Sc_2O@T_d(19151)$-C_{76}[28] Obtained in (n-Bu_4N)(PF_6)/o-DCB with Ferrocene as the Internal Standard

compd	$E^{2+/+}$	$E^{+/0}$	$E^{0/-}$	$E^{-/2-}$	$E^{2-/3-}$	$E^{3-/4-}$	$E^{4-/5-}$	$E_{gap,ec}$ (V)
$Sc_2O@C_{2v}(5)$-C_{80}	+0.56[a]	+0.24[a]	−0.89[b]	−1.48[b]	−1.75[b]	−1.96[b]	−2.13[b]	1.13
$Sc_2C_2@C_{2v}(5)$-C_{80}		+0.41[c]	−0.74[c]	−1.33[c]				1.15
$Sc_2O@C_s(6)$-C_{82}	+0.72[a]	+0.35[a]	−0.96[a]	−1.28[a]	−1.74[b]			1.31
$Sc_2S@C_s(6)$-C_{82}	+0.65[a]	+0.39[a]	−0.98[a]	−1.12[a]	−1.73[b]			1.37
$Sc_2O@T_d(19151)$-C_{76}		+0.32[a]	−0.91[a]	−1.40[b]	−1.65[b]	−1.93[b]	−2.30[b]	1.23

[a]Half-wave potential in volts (reversible redox process). [b]Peak potential in volts (irreversible redox process). [c]Differential pulse voltammetry potential in volts.

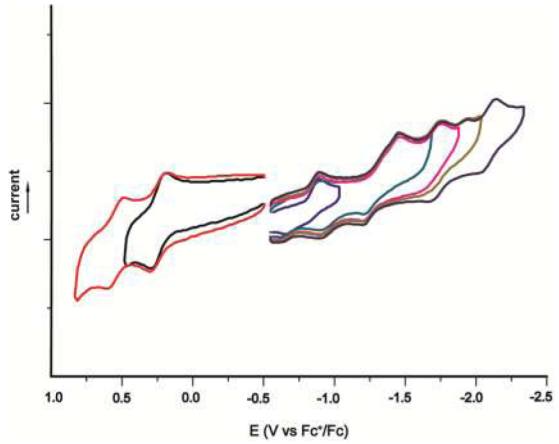

Figure 5. Cyclic voltammograms of $Sc_2O@C_{2v}(5)$-C_{80} in $TBAPF_6$/o-DCB with ferrocene as the internal standard, 100 mV s^{-1} scan rate.

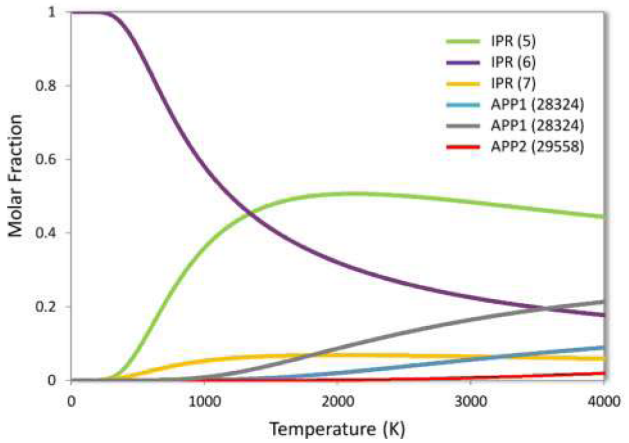

Figure 6. Predicted molar fractions of the lowest-energy $Sc_2O@C_{80}$ isomers as a function of the temperature using the free-encapsulating model (FEM).

Table 2. Relative Energies (in kcal mol^{-1}) for the Selected Isomers of C_{80} in the Tetra-Anion and Endohedral Forms[a]

isomer	sym	APP[b]	C_{80}^{4-}	$Sc_2O@C_{80}$
6	D_{5h}	0	4.2	0.0
5	C_{2v}	0	10.4	3.2
7	I_h	0	0.0	4.0
31876	C_1	1	32.9	11.6
28324	C_1	1	32.7	16.9
31891	C_1	1	32.1	27.4
29558	C_1	2	42.6	29.4
3	C_{2v}	0	33.8	31.4
31911	C_{2v}	1	36.5	31.9
4	D_3	0	41.9	32.8

[a]Isome number according to the spiral algorithm of Fowler and Manolopoulos.[32] The truncated numbering is used for the IPR isomers. [b]APP: number of adjacent pentagon pairs.

found for the most stable and characterized cluster fullerenes (Figure S3).[20,31]

Since the energy differences between the different isomers are small, the effect of the higher temperatures at which fullerenes are formed can be critical to determine their relative stabilities and abundances. Hence, we have also computed the molar fractions of these isomers as a function of the temperature (0−4000 K) using the rigid rotor and harmonic oscillator approximation combined with the related free-encapsulating model (FEM) as proposed by Slanina (Figure 6).[33,34] The two most abundant isomers are $Sc_2O@D_{5h}(6)$-C_{80} and $Sc_2O@C_{2v}(5)$-C_{80}, which are related by a single Stone−Wales transformation (see Figure S4).[32] $Sc_2O@D_{5h}(6)$-C_{80} dominates at temperatures lower than 1300 K, but $Sc_2O@C_{2v}(5)$-C_{80} becomes the most abundant isomer at higher temperatures (T > 1300 K). Thus, thermal and entropic contributions are relevant to rationalize the relative abundances of this family of OCFs, i.e., that the $Sc_2O@C_{2v}(5)$-C_{80} isomer is the one observed in the experiments.

The optimized structures of isomers $Sc_2O@C_{2v}(5)$-C_{80}, $Sc_2O@D_{5h}(6)$-C_{80}, and $Sc_2O@I_h(7)$-C_{80} are shown in Figure 7. For $Sc_2O@C_{2v}(5)$-C_{80}, the Sc−O distances are 1.90 Å for Sc1 and 1.93 Å for Sc2, and the Sc1−O−Sc2 angle is 164.2°, in rather good agreement with the X-ray data.

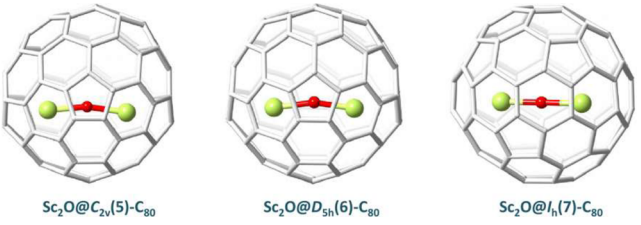

Figure 7. Optimized structures of $Sc_2O@C_{2v}(5)$-C_{80}, $Sc_2O@D_{5h}(6)$-C_{80}, and $Sc_2O@I_h(7)$-C_{80}.

We have also performed Car−Parrinello molecular dynamics simulations at room temperature and at a higher temperature nearer to conditions of fullerene formation (2000 K) for $Sc_2O@C_{2v}(5)$-C_{80}. We have seen that, at 2000 K, the Sc_2O unit is moving rather freely inside the fullerene cage (Figure 8), as supposed by the FEM model. At room temperature, we observe significant motion of the cluster at the short time scale of the simulations (see Figure S5), which makes us infer that free rotation is operative on the NMR time scale. The variations of the Sc1−O−Sc2 angle at room temperature and 2000 K during

DOI: 10.1021/acs.inorgchem.5b01613
Inorg. Chem. 2015, 54, 9845−9852

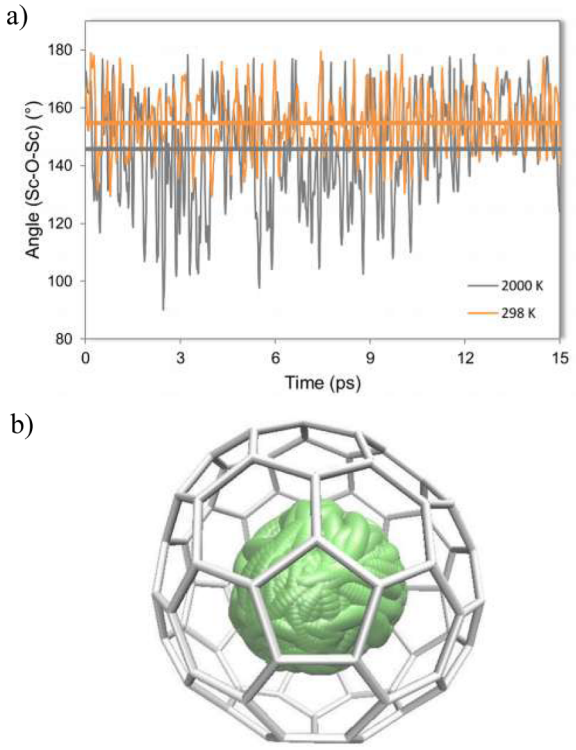

Figure 8. (a) Variations of the Sc1−O−Sc2 angle along the trajectory at room temperature (orange) and 2000 K (gray). The average of the angle is 155° at 298 K and 146° at 2000 K. The standard deviations are 10° and 17°, respectively. (b) Motion of the Sc_2O cluster inside the $C_{2v}(5)$-C_{80} cage during the simulation at 2000 K.

about 15 ps are represented in Figure 8a. Oscillations of the angle are much more important at higher temperature.

From an analysis of the frontier molecular orbitals, we have confirmed that there is a formal transfer of four electrons from the Sc_2O unit to the C_{80} cage, i.e., $(Sc_2O)^{4+}@(C_{80})^{4-}$ (see Figure 9). The HOMO and LUMO are mainly localized on the C_{80} framework, so the first oxidation and reduction take place in the cage. Therefore, the electronic structure can be explained

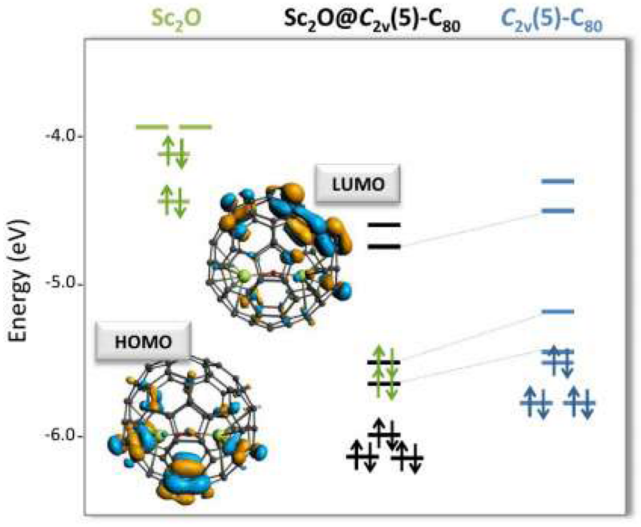

Figure 9. Orbital interaction diagram for $Sc_2O@C_{2v}(5)$-C_{80}. The fragments Sc_2O and $C_{2v}(5)$-C_{80} are calculated with the geometry that they have in the OCF.

by the ionic model with a formal transfer of four electrons from the cluster to the cage.

We have computed the oxidation and reduction potentials for the $Sc_2O@C_{2v}(5)$-C_{80} and $Sc_2O@D_{5h}(6)$-C_{80} isomers (Table S1). The computed HOMO−LUMO gaps are found to be 0.794 and 0.293 eV, respectively. The computed electrochemical (EC) gaps are 1.163 eV for isomer 5 and 0.697 eV for isomer 6. The results for $Sc_2O@C_{2v}(5)$-C_{80} are in much better agreement with the experimental ones than those for $Sc_2O@D_{5h}(6)$-C_{80}, the other isomer that is predicted to have a non-negligible abundance at high temperatures.

We have also computed the UV−vis−NIR spectrum using time-dependent (TD) DFT for these two most abundant isomers. The experimental absorption spectrum of $Sc_2O@C_{80}$ is shown in Figure 3. Experimental transitions are obtained at 538−596, 656, and 766−850 nm. The predicted spectra for both isomers are displayed in Figure S6a and Figure S6b. The spectrum computed for $Sc_2O@C_{2v}(5)$-C_{80} compares rather well with the experimental one. We have found the following transitions (see Figure S6a): 643, 683, 915, 967, 1017, 1199, and 1453 nm. On the other hand, the predicted transitions for $Sc_2O@D_{5h}(6)$-C_{80} (see Figure S6b) are 522, 527, 1348, 1692, 1825, and 1884 nm.

All the results confirm $Sc_2O@C_{2v}(5)$-C_{80} as the isolated OCF with formula $Sc_2O@C_{80}$. The other predicted isomer with lower abundance would be $Sc_2O@D_{5h}(6)$-C_{80}, but it shows a very low HOMO−LUMO gap and, consequently, very low kinetic stability, which makes it more difficult to isolate in case it formed. It is true that both the experimental electrochemical properties and UV−vis−NIR spectrum for $Sc_2O@C_{80}$ and $Sc_2C_2@C_{2v}(5)$-C_{80} show some differences, but they should be due to the different encapsulated cluster. The differences in the first oxidation and reduction potentials for $Sc_2O@C_{2v}(5)$-C_{80} and $Sc_2C_2@C_{2v}(5)$-C_{80} (around 150 mV) are larger than for other cluster fullerenes that share the same cage (usually the differences are less than 100 mV, see Table S3). Since the two peaks are shifted the same value, the EC gap is almost the same for the oxide and the carbide CFs. Regarding their UV−vis−NIR spectra, the most significant features for the two CFs are reproduced by computations, in particular the spectral onset and the characteristic features between 600 and 700 nm.

Same $C_{2v}(5)$-C_{80} Cage, but Different Cluster: Sc_2O vs Sc_2C_2. To this end, we find that the DFT-optimized structure of $Sc_2O@C_{2v}(5)$-C_{80} is very close to that of the X-ray model shown in Figure 2, suggesting that both of them point to the absolute structure of $Sc_2O@C_{2v}(5)$-C_{80}. Furthermore, it is informative to compare the Sc_2O unit in $Sc_2O@C_{2v}(5)$-C_{80}·[Ni^{II}(OEP)] with the already reported Sc_2C_2 unit in $Sc_2C_2@C_{2v}(5)$-C_{80}·[Ni^{II}(OEP)] since either unit is rather fixed inside the corresponding $C_{2v}(5)$-C_{80} cage.[29] A close observation reveals that the positions of the two major Sc sites in $Sc_2O@C_{2v}(5)$-C_{80}·[Ni^{II}(OEP)] are almost identical: each site approaches the [6,6] bond of a pyracylene unit (fused six-membered rings with abutted pentagons) with the shortest Sc-cage contacts ranging from 2.23 to 2.25 Å. However, it shows differences from the previous observation of $Sc_2C_2@C_{2v}(5)$-C_{80}·[Ni^{II}(OEP)], in which one Sc atom is close to the [6,6] bond whereas the other approaches a hexagonal ring.[29] This observation is also consistent with the above-mentioned differences on their ^{45}Sc NMR spectra and suggests that, despite the close resemblance between the electronic structures of these two molecules, subtle differences do exist on their

DOI: 10.1021/acs.inorgchem.5b01613
Inorg. Chem. 2015, 54, 9845−9852

crystal structures as well as the interactions between the clusters and corresponding cages.

On the other hand, despite the minor differences for both $Sc_2O@C_{2v}(5)$-C_{80}·[Ni^{II}(OEP)] and $Sc_2C_2@C_{2v}(5)$-C_{80}·[Ni^{II}(OEP)], the two Sc atoms within each cluster are still in the vicinity of pyracylene units. This might indicate that, for these dimetallic cluster fullerenes, there is a significant interaction between the metal and pyracylene unit. In fact, for $C_{2v}(5)$-C_{80}, 10 out of the 12 pentagons, which are the faces that concentrate the negative charge,[31] are involved in the 9 pyracylene units that are present in the structure. The computed molecular electrostatic potential (MEP, see SI) for the cage tetra-anion shows that, for both the Sc_2O and Sc_2C_2 clusters, one of the Sc ions binds to the most nucleophilic pyracylene unit and the second Sc ion is placed near other pyracylene while preserving the structure of the cluster. It thus confirms the remarkable ionic (electron transfer) interactions between the metals and the pyracylene units, which combine with the non-negligible covalent interactions also present in these OCFs.[9]

■ CONCLUSIONS

A new oxide cluster fullerene $Sc_2O@C_{2v}(5)$-C_{80} has been isolated and characterized by mass spectrometry, UV−vis−NIR absorption spectroscopy, cyclic voltammetry, ^{45}Sc NMR, DFT calculations, and single crystal X-ray diffraction. The crystallographic analysis unambiguously assigned the cage symmetry to $C_{2v}(5)$-C_{80} and suggests that the Sc_2O cluster is ordered inside the cage. The comparative crystallographic analysis between $Sc_2O@C_{2v}(5)$-C_{80} and other dimetallic cluster fullerenes shows that the endohedral Sc_2O unit demonstrates notable flexibility and displays large variation in the Sc−O−Sc angle, dictated by the size and shape of the cages. Further studies also reveal the subtle differences existing on the crystal structures as well as the interactions between the clusters and corresponding cages of the $Sc_2O@C_{2v}(5)$-C_{80} and $Sc_2C_2@C_{2v}(5)$-C_{80} despite their structural resemblance. In addition, the spectroscopic and electrochemical studies show that, though they share the same $C_{2v}(5)$-C_{80} cage, the internal clusters of Sc_2O and Sc_2C_2 exert a significant impact on the spectroscopic and electrochemical properties as well as on their electronic structures. Computational analysis shows that there is a formal transfer of four electrons from the Sc_2O unit to the C_{80} cage, i.e., $(Sc_2O)^{4+}@(C_{80})^{4-}$, and the HOMO and LUMO are mainly localized on the C_{80} framework. Moreover, $Sc_2O@C_{2v}(5)$-C_{80} is predicted to be the most abundant thermodynamic isomer at high temperatures (T > 1300 K), in agreement with the X-ray characterization, thus confirming again the relevant role that thermal and entropic effects play in the relative stabilization of OCFs.

■ EXPERMENTAL SECTION

Preparation and Isolation of $Sc_2O@C_{2v}(5)$-C_{80}. The carbon soot containing OCFs was synthesized using an improved arc-discharge method.[35−38] Graphite rods were packed with a 20:1 molar ratio of graphite powders and Sc_2O_3 powders. The prepared graphite rods were then burned in the arcing chamber under a 200 Torr of helium and 20 Torr of CO_2 atmosphere. The as-produced soot was extracted with chlorobenzene. The extract was further subjected to a multistage HPLC (Japan Analytical Industry Co., Ltd.) procedure to isolate and purify $Sc_2O@C_{2v}(5)$-C_{80} with toluene as mobile phase at the flow rate of 4.0 mL/min. The UV detector was set to 340 nm for fullerene detection and a combination of 20 mm × 250 mm Buckyprep-M columns (Nacalai Tesque, Japan), 10 mm × 250 mm Buckyprep columns (Nacalai Tesque, Japan), and 10 mm × 250 mm 5PBB columns (Nacalai Tesque, Japan) was utilized in these procedures. The purity of the isolated product was further checked by HPLC using a 10 mm × 250 mm Buckyprep column (Nacalai Tesque, Japan) with the flow rate of 4.0 mL/min. The corresponding MALDI-TOF (Ultraflextreme, Bruker, Germany) data for the isolated product is shown in Figure 1.

UV−Vis−NIR Studies of $Sc_2O@C_{2v}(5)$-C_{80}. The UV−vis−NIR spectrum was measured on a UV-3600 spectrometer (Shimadzu, Japan) with the $Sc_2O@C_{2v}(5)$-C_{80} dissolved in carbon disulfide.

Electrochemical Studies of $Sc_2O@C_{2v}(5)$-C_{80}. Cyclic voltammetry was performed in *o*-dichlorobenzene containing 0.05 M $TBAPF_6$ as supporting electrolyte, using glassy carbon disk as the working electrode with a Zennium Electrochemical Workstation (Zahner, Germany). The scan rate of CV was 100 mV/s.

Computational Studies of $Sc_2O@C_{80}$. We have computed all the tetra-anions of C_{80} with two or fewer adjacent pentagon pairs (APP) using density functional theory (DFT) methodology with the ADF 2012 program.[39,40] The exchange-correlation functional of Becke and Perdew (BP86) and the Slater TZP basis sets were used.[41,42] The lowest-energy tetra-anionic cages (less than ∼40 kcal·mol^{-1}) were selected, and the corresponding structures of $Sc_2O@C_{80}$ were optimized at the same level of theory. We have computed the UV−vis−NIR spectrum for $Sc_2O@C_{2v}(5)$-C_{80} and $Sc_2O@D_{5h}(6)$-C_{80} using time-dependent (TD) DFT in the vis−NIR region, for wavelengths larger than 500 nm (at BP86/TZP level). Molecular dynamics simulations were carried out using Car−Parrinello Molecular Dynamics (CPMD) program.[43] The description of the electronic structure was based on the expansion of the valence electronic wave functions into a plane wave basis set, which was limited by an energy cutoff of 70 Ry. The interaction between the valence electrons and the ionic cores was treated through the pseudopotential (PP) approximation (Martins−Troullier type).[44] The functional by Perdew, Burke, and Ernzerhoff (PBE) was selected as density functional.[45,46] We included the nonlinear core corrections (NLCC) in the Martins−Troullier PP for scandium atom.[47] The simulations were carried out using periodic boundary conditions in a cubic cell with a side length of 15 Å, a fictitious electron mass of 800 au, and a time step of 0.144 fs.

Single Crystal X-ray Diffraction Analysis. Black cocrystals of $Sc_2O@C_{2v}(5)$-C_{80}·[Ni^{II}(OEP)] were obtained by allowing the benzene solution of fullerene and the chloroform solution of [Ni^{II}(OEP)] to diffuse together. X-ray data were collected at 123 K using a diffractometer (APEX II; Bruker Analytik GmbH) equipped with a CCD collector. Multiscan method was used for absorption correction. The structure was resolved using direct methods (SHELXS97) and refined on F^2 using full-matrix least-squares using SHELXL97.[48] Hydrogen atoms were added geometrically and refined with a riding model. Co-crystal of $Sc_2O@C_{2v}(5)$-C_{80}·[Ni^{II}(OEP)] contains another severely disordered lattice of C_6H_6 and $CHCl_3$ molecules that could not be modeled properly. Therefore, program SQUEEZE, a part of the PLATON package of crystallographic software,[49,50] was used to calculate the solvent disorder area and remove its contribution from the intensity data.

Crystal Data for $Sc_2O@C_{2v}(5)$-C_{80}·[Ni^{II}(OEP)]·0.76C_6H_6·0.24$CHCl_3$. $C_{120.75}H_{48.75}Cl_{0.75}N_4NiOSc_2$, M_r = 1746.61, 0.20 × 0.18 × 0.15 mm^3, monoclinic, $C2/m$ (No. 12), a = 25.3547(5) Å, b = 15.1067(3) Å, c = 19.5200(4) Å, β = 94.502(1)°, V = 7453.6(3) Å^3, Z = 4, ρ_{calcd} = 1.556 g cm^{-3}, μ(Mo Kα) = 0.522 mm^{-1}, θ = 2.57−27.58°, T = 123 K, R1 = 0.0773, wR2 = 0.2084 for all data; R1 = 0.0713, wR2 = 0.2041 for 7895 reflections (I > 2.0σ(I)) with 1272 parameters. Goodness of fit indicator 1.016. Maximum residual electron density 1.010 e Å^{-3}.

■ ASSOCIATED CONTENT

Supporting Information

The Supporting Information is available free of charge on the ACS Publications website at DOI: 10.1021/acs.inorgchem.5b01613.

DOI: 10.1021/acs.inorgchem.5b01613
Inorg. Chem. 2015, 54, 9845−9852

HPLC chromatograms and complementary computational results (PDF)
X-ray crystallographic details for $Sc_2O@C_{2v}(5)$-C_{80} (CIF)

AUTHOR INFORMATION

Corresponding Authors

*E-mail: antonio.rodriguezf@urv.cat.
*E-mail: josepmaria.poblet@urv.cat.
*E-mail: fenglai@suda.edu.cn.
*E-mail: chenning@suda.edu.cn.

Author Contributions

Q.T. and L.A. contributed equally to this work.

Notes

The authors declare no competing financial interest.

ACKNOWLEDGMENTS

We cordially thank Prof. Shuao Wang and Dr. Daopeng Sheng (Soochow University) for the kind help with the single crystal X-ray diffraction measurements. This work is supported in part by the NSFC (21241004, 51372158, 21305098, and 51302178), SRFDP (20123201120014), the NSF of Jiangsu Province (BK2012611 and BK20130295), Jiangsu Specially Appointed Professor Program (SR10800113), the Project for Jiangsu Scientific and Technological Innovation Team (2013), and the Priority Academic Program Development of Jiangsu Higher Education Institutions (PAPD). This work was also supported by the Spanish Ministerio de Ciencia e Innovación (Project CTQ2014-52774-P) and by the Generalitat de Catalunya (2014SGR-199 and XRQTC). L.A. thanks the Generalitat de Catalunya for a predoctoral fellowship (FI-DGR 2014).

REFERENCES

(1) Kroto, H. W.; Heath, J. R.; O'Brien, S. C.; Curl, R. F.; Smalley, R. E. *Nature* **1985**, *318*, 162−163.
(2) Shinohara, H. *Rep. Prog. Phys.* **2000**, *63*, 843−892.
(3) Lu, X.; Bao, L. P.; Akasaka, T.; Nagase, S. *Chem. Commun.* **2014**, *50*, 14701−14715.
(4) Garcia-Borras, M.; Osuna, S.; Luis, J. M.; Swart, M.; Sola, M. *Chem. Soc. Rev.* **2014**, *43*, 5089−5105.
(5) Rivera-Nazario, D. M.; Pinzon, J. R.; Stevenson, S.; Echegoyen, L. A. *J. Phys. Org. Chem.* **2013**, *26*, 194−205.
(6) Yang, S. F. *Curr. Org. Chem.* **2012**, *16*, 1079−1094.
(7) Lu, X.; Feng, L.; Akasaka, T.; Nagase, S. *Chem. Soc. Rev.* **2012**, *41*, 7723−7760.
(8) Yang, S.; Liu, F.; Chen, C.; Jiao, M.; Wei, T. *Chem. Commun.* **2011**, *47*, 11822−11839.
(9) Popov, A. A.; Yang, S.; Dunsch, L. *Chem. Rev.* **2013**, *113*, 5989−6113.
(10) Cardona, C. M. *Curr. Org. Chem.* **2012**, *16*, 1095−1108.
(11) Akasaka, T.; Lu, X. *Chem. Rec.* **2012**, *12*, 256−269.
(12) Dreiser, J.; Westerström, R.; Zhang, Y.; Popov, A. A.; Dunsch, L.; Krämer, K.; Liu, S.-X.; Decurtins, S.; Greber, T. *Chem. - Eur. J.* **2014**, *20*, 13536−13540.
(13) Yang, S. *Curr. Org. Chem.* **2012**, *16*, 1079−1094.
(14) Lu, X.; Bao, L.; Akasaka, T.; Nagase, S. *Chem. Commun.* **2014**, *50*, 14701−14715.
(15) Popov, A. A.; Chen, N.; Pinzón, J. R.; Stevenson, S.; Echegoyen, L. A.; Dunsch, L. *J. Am. Chem. Soc.* **2012**, *134*, 19607−19618.
(16) Wu, B.; Wang, T.; Feng, Y.; Zhang, Z.; Jiang, L.; Wang, C. *Nat. Commun.* **2015**, *6*, 6468.
(17) Rodriguez-Fortea, A.; Balch, A. L.; Poblet, J. M. *Chem. Soc. Rev.* **2011**, *40*, 3551−3563.
(18) Martin, N. *Chem. Commun.* **2006**, 2093−2104.
(19) Popov, A. A.; Dunsch, L. *J. Am. Chem. Soc.* **2007**, *129*, 11835−11849.
(20) Rodriguez-Fortea, A.; Poblet, J. M. *Faraday Discuss.* **2014**, *173*, 201−213.
(21) Wang, T.; Wang, C. *Acc. Chem. Res.* **2014**, *47*, 450−458.
(22) Kurihara, H.; Lu, X.; Iiduka, Y.; Mizorogi, N.; Slanina, Z.; Tsuchiya, T.; Akasaka, T.; Nagase, S. *J. Am. Chem. Soc.* **2011**, *133*, 2382−2385.
(23) Valencia, R.; Rodriguez-Fortea, A.; Stevenson, S.; Balch, A. L.; Poblet, J. M. *Inorg. Chem.* **2009**, *48*, 5957−5961.
(24) Stevenson, S.; Mackey, M. A.; Stuart, M. A.; Phillips, J. P.; Easterling, M. L.; Chancellor, C. J.; Olmstead, M. M.; Balch, A. L. *J. Am. Chem. Soc.* **2008**, *130*, 11844−11845.
(25) Mercado, B. Q.; Olmstead, M. M.; Beavers, C. M.; Easterling, M. L.; Stevenson, S.; Mackey, M. A.; Coumbe, C. E.; Phillips, J. D.; Phillips, J. P.; Poblet, J. M.; Balch, A. L. *Chem. Commun.* **2010**, *46*, 279−281.
(26) Mercado, B. Q.; Stuart, M. A.; Mackey, M. A.; Pickens, J. E.; Confait, B. S.; Stevenson, S.; Easterling, M. L.; Valencia, R.; Rodriguez-Fortea, A.; Poblet, J. M.; Olmstead, M. M.; Balch, A. L. *J. Am. Chem. Soc.* **2010**, *132*, 12098−12105.
(27) Zhang, M.; Hao, Y.; Li, X.; Feng, L.; Yang, T.; Wan, Y.; Chen, N.; Slanina, Z.; Uhlík, F.; Cong, H. *J. Phys. Chem. C* **2014**, *118*, 28883−28889.
(28) Yang, T.; Hao, Y.; Abella, L.; Tang, Q.; Li, X.; Wan, Y.; Rodríguez-Fortea, A.; Poblet, J. M.; Feng, L.; Chen, N. *Chem. - Eur. J.* **2015**, *21*, 11110−11117.
(29) Kurihara, H.; Lu, X.; Iiduka, Y.; Nikawa, H.; Hachiya, M.; Mizorogi, N.; Slanina, Z.; Tsuchiya, T.; Nagase, S.; Akasaka, T. *Inorg. Chem.* **2012**, *51*, 746−750.
(30) Mercado, B. Q.; Chen, N.; Rodríguez-Fortea, A.; Mackey, M. A.; Stevenson, S.; Echegoyen, L.; Poblet, J. M.; Olmstead, M. M.; Balch, A. L. *J. Am. Chem. Soc.* **2011**, *133*, 6752−6760.
(31) Rodríguez-Fortea, A.; Alegret, N.; Balch, A. L.; Poblet, J. M. *Nat. Chem.* **2010**, *2*, 955−961.
(32) Fowler, P. W.; Manolopoulos, D. E. *An Atlas of Fullerenes*; Oxford University Press: Oxford, U.K., 1995.
(33) Slanina, Z.; Nagase, S. *ChemPhysChem* **2005**, *6*, 2060−2063.
(34) Slanina, Z.; Lee, S.-L.; Uhlík, F.; Adamowicz, L.; Nagase, S. *Theor. Chem. Acc.* **2007**, *117*, 315−322.
(35) Kratschmer, W.; Lamb, L. D.; Fostiropoulos, K.; Huffman, D. R. *Nature* **1990**, *347*, 354−358.
(36) Johnson, R. D.; de Vries, M. S.; Salem, J.; Bethune, D. S.; Yannoni, C. S. *Nature* **1992**, *355*, 239−240.
(37) Kikuchi, K.; Suzuki, S.; Nakao, Y.; Nakahara, N.; Wakabayashi, T.; Shiromaru, H.; Saito, K.; Ikemoto, I.; Achiba, Y. *Chem. Phys. Lett.* **1993**, *216*, 67−71.
(38) Bethune, D. S.; Johnson, R. D.; Salem, J. R.; de Vries, M. S.; Yannoni, C. S. *Nature* **1993**, *366*, 123−128.
(39) te Velde, G.; Bickelhaupt, F. M.; Baerends, E. J.; Fonseca Guerra, C.; van Gisbergen, S. J. A.; Snijders, J. G.; Ziegler, T. *J. Comput. Chem.* **2001**, *22*, 931.
(40) Baerends, E. J.; Ellis, D. E.; Ros, P. *ADF 2012.01*; Department of Theoretical Chemistry, Vrije Universiteit: Amsterdam, 2012.
(41) Becke, A. D. *Phys. Rev. A: At., Mol., Opt. Phys.* **1988**, *38*, 3098−3100.
(42) Becke, A. D. *J. Chem. Phys.* **1986**, *84*, 4524−4529.
(43) Car, R.; Parrinello, M. *Phys. Rev. Lett.* **1985**, *55*, 2471−2474.
(44) Troullier, N.; Martins, J. L. *Phys. Rev. B: Condens. Matter Mater. Phys.* **1991**, *43*, 1993−2006.
(45) Perdew, J. P.; Burke, K.; Ernzerhof, M. *Phys. Rev. Lett.* **1996**, *77*, 3865−3868.
(46) Perdew, J. P.; Burke, K.; Ernzerhof, M. *Phys. Rev. Lett.* **1997**, *78*, 1396−1396.
(47) Louie, S. G.; Froyen, S.; Cohen, M. L. *Phys. Rev. B: Condens. Matter Mater. Phys.* **1982**, *26*, 1738−1742.
(48) Sheldrick, G. M. *Acta Crystallogr., Sect. A: Found. Crystallogr.* **2008**, *64*, 112−122.

DOI: 10.1021/acs.inorgchem.5b01613
Inorg. Chem. 2015, 54, 9845−9852

(49) Spek, A. L. *PLATON. A Multipurpose Crystallographic Tool*; Utrecht University: Utrecht, The Netherlands, 2003.
(50) van der Sluis, P.; Spek, A. L. *Acta Crystallogr., Sect. A: Found. Crystallogr.* **1990**, *46*, 194−201.

DOI: 10.1021/acs.inorgchem.5b01613
Inorg. Chem. 2015, 54, 9845−9852